Validation of a finite element model in ANSYS WorkBench for IsoTruss® structures in uniaxial compression

Hanna B. Opdahl* and David W. Jensen†
Brigham Young University‡, Provo, UT, 84602

The purpose of this study was to develop, verify, and validate a finite element (FE) model of IsoTruss® structures subject to uniaxial compression. The FE model was developed in ANSYS WorkBench and verified using axial stiffness and critical buckling loads that were calculated from traditional mechanics. The buckling failure modes include global buckling and local/shell-like buckling. The predictions from the FE model and mechanics calculations are validated by experimental data generated in preceding studies. Results indicate that the effective material modulus is highly affected by variations in manufacturing. The FE models correlate with the axial stiffness and critical buckling loads demonstrated in experimental testing when the nominal material properties are adjusted to account for: imperfections in manufacturing; imperfections in material properties; and/or, the limitations of micromechanics equations. The FE model developed in this study is used in subsequent research to perform dimensional analyses and analyze novel configurations of IsoTruss structures that have not been manufactured or tested experimentally.

I. Nomenclature

A_i	Cross-sectional area of longitudinal (L) or helical (H) member
A_t	Cross-sectional area of carbon fiber tow
D	Outer diameter of IsoTruss
D_X	Equivalent plate flexural rigidity of planar X-style helical trusses
E_i	Effective buckling (b) or stiffness (s) modulus
E_t	Young's modulus of constituent in tension
E_X	Equivalent plate stiffness of planar X-style helical trusses in the z-direction
E_z	Young's modulus of composite in z-direction
G	Shear modulus
I_i	Moment of inertia of global IsoTruss (g) or a single longitudinal member (L)
K_z	Axial stiffness of structure in the z-direction
L	Length of global IsoTruss
N	Number of nodes
N_b	Number of bays
N_{t_i}	Number of fiber tows per longitudinal (L) or helical (H) member
P_i	Buckling load of global (g) or shell-like (sb) buckling mode
R	Outer radius of IsoTruss
b	Bay length (one repeating unit consisting of a planar X-style truss and a pyramid)
c	Moment of inertia coefficient [1]
l_1	Short span of longitudinal member between transition nodes
r_i	Radius of longitudinal (L) or helical (H) member
v_f	Fiber volume fraction
δ_2	One-half the base length of the planar X-style helical members
δ_{max}	Maximum axial deflection of global IsoTruss
ϕ	Inclination angle of helical members from horizontal
γ	Localized rotation of longitudinal strut within a bay
λ	Load multiplier for eigenvalue buckling

*Graduate Research Assistant, Dept. of Civil and Environmental Engineering, 430EB Brigham Young University.
†Professor, Dept. of Civil and Environmental Engineering, 430EB Brigham Young University.

μ_i	Boundary constraint coefficient of global (g) or shell-like (sb) buckling (converts length to effective length)
ν	Poisson's ratio
ρ	Material density
θ	Configuration reference angle ($360°/N$)

II. Introduction

IsoTruss® grid columns are open-lattice composite structures that have been designed and manufactured for diverse applications from civil infrastructure to aerospace structures. The structural configuration is designed to maximize structural efficiency by aligning longitudinal and helical members with anticipated loading scenarios [2]. The longitudinal members are straight, continuous members that span the global length, primarily providing flexural and axial strength. Helical members wind around the structure employing piece-wise linear segments to form a continuous helical-like member and provide torsional rigidity, shear resistance, and lateral stability to the longitudinal members.

Various configurations of IsoTruss structures have been developed and tested experimentally in preceding research. While experimental studies are reliable in demonstrating the actual failure modes of the structure, they can be expensive and time consuming, only producing one set of data. Finite element (FE) analysis is a highly robust, numerical method to assess the structural performance and capacity of untested configurations of IsoTruss structures. FE methods allow new designs to be assessed quickly and inexpensively, without the need to manufacture and physically load each configuration. Before performing an FE analysis, the FE model must be validated with experimental data and verified with traditional mechanics to ensure accurate results.

The purpose of the current study is to develop an FE model, validate it with experimental data gathered in preceding studies, and verify the results with traditional mechanics calculations. The scope of this study is limited to graphite/epoxy IsoTruss structures with 8-nodes and subject to uniaxial compression. The configurations are designed with longitudinal members at the inner diameter of the structure. Typical failure modes include material failure, global buckling, and local/shell-like buckling. The FE model is validated with experimental data including the axial deflection and critical buckling loads of the specimens that were manufactured and tested by McCune [3] and Rackliffe et al. [4].

III. Background

Rackliffe et al. and McCune constructed carbon/epoxy IsoTruss structures to test under uniaxial compression. Both studies manufactured the specimens by consolidating the members at the nodes with spiral-wrapping. Rackliffe et al. tested four long IsoTruss structures with 8-nodes to determine the critical buckling loads, whereas McCune analyzed both 6- and 8-node configurations that were shorter and failed by crushing. McCune and Rackliffe et al. present the total deformation and ultimate load of each specimen. The specimens tested by Rackliffe et al. failed in local/shell-like buckling and global buckling, thereby providing critical buckling loads to validate eigenvalue buckling models. The data of McCune and Rackliffe et al. are used in the current study to validate the FE model with experimental results.

Sui et al. [5] developed an FE model of IsoTruss structures with Patran Command Language that is verified with theoretical equations derived from traditional mechanics. The IsoTruss structures were modeled with 8-nodes to correspond with the experiments performed by Rackliffe et al. The model incorporates four potential failure modes previously observed in experiments and FE models: fracture of the struts, global buckling, shell-like buckling, and mono-cell buckling. Mono-cell buckling is the buckling of longitudinal members at the bay-level and is referred to herein as longitudinal strut buckling. Opdahl [6] re-derives the shell-like buckling equation of Sui et al. from energy methods, with slight variations discussed therein. The resulting expression is implemented in the current chapter to compare the analytical predictions with the FE predictions. Global buckling and axial deflection are predicted analytically with the traditional equations for column buckling and stiffness, respectively.

IV. Methods

This section outlines the procedure for developing, verifying, and validating the FE model. The nominal material properties of the composite were calculated from the fiber and matrix properties documented by Rackliffe et al. and McCune. The geometry of each structure was drafted in ANSYS SpaceClaim. Static structural analyses were performed on each unique configuration to predict the axial stiffness. The results are verified with mechanics calculations and validated with the axial stiffness reported from the physical testing. The nominal modulus of the composite is reduced to an effective modulus to correlate the model with the experimental results.

Once the axial stiffness predictions from ANSYS were verified with mechanics and correlated with the experimental data, eigenvalue buckling analyses were performed for each of the specimens tested by Rackliffe et al. The global and shell-like buckling loads predicted by the FE

models are verified with the Euler buckling equation and the shell-like buckling equation [6], respectively. The nominal material modulus is adjusted to an effective buckling material modulus and re-analyzed to correlate the model with the experimental results.

The specimens that were tested by Rackliffe et al. are referred to throughout this paper as Rackliffe1, Rackliffe2, Rackliffe3, and Rackliffe4. They correspond to the specimens referred to by Rackliffe et al. as IsoTruss1, IsoTruss2, IsoTruss3, and IsoTruss4, respectively. Likewise, the specimens that were manufactured by McCune are referred to in this paper as McCune8, McCune12, McCune16, and McCune20. They correspond to the specimens manufactured by McCune with 8, 12, 16, and 20 carbon fiber tows in the longitudinal members.

A. Composite Material Properties

Tables 1 and 2 present the material properties of the carbon fiber and resin used by McCune [3] and Rackliffe et al. [4], respectively, to manufacture the physical specimens for experimental testing. Poisson's ratio was not documented in the publications, therefore, the values shown below were selected based on the material properties of similar materials.

Table 1 Material Properties (McCune [3])

	Carbon Fiber	Resin
Name	Thornel 12K T300C	EPON 826
E_t [ksi (GPa)]	33000 (228)	400 (2.76)
ν	0.32	0.33
$\rho \left[\frac{\text{lb.}}{\text{in.}^3} \left(\frac{\text{kg}}{\text{m}^3}\right)\right]$	0.063 (1750)	0.042 (1162)

Table 2 Material Properties (Rackliffe [7])

	Carbon Fiber	Resin
Name	IM7 6K	UF3325-95
E_t [ksi (GPa)]	40000 (276)	410 (2.83)
ν	0.32	0.33
$\rho \left[\frac{\text{lb.}}{\text{in.}^3} \left(\frac{\text{kg}}{\text{m}^3}\right)\right]$	0.064 (1780)	0.044 (1207)
$A_t \left[\text{in.}^2 \left(\text{mm}^2\right)\right]$	1.94e-04 (0.125)	-

The material properties of the fiber and resin provided in Tables 1 and 2 were used to calculate the orthotropic material properties of the composite using the micromechanics equations presented by Kollar and Springer [8]. Since McCune and Rackliffe et al. only provide the *tensile* modulus of the carbon fiber, the *compression* modulus was approximated by applying the compressive-to-tensile stiffness ratio of a HexTow IM7 composite to the fiber tensile modulus. The resulting material properties of the composites are provided in Table 3.

B. Geometry

Table 4 presents the geometric properties of the experimental specimens prepared by McCune and Rackliffe et al. that are used to draft the model geometry in ANSYS SpaceClaim. The radii of the McCune specimens are based on the axial area and the fiber volume fractions reported by McCune.

Table 3 Nominal Properties of Composite Materials

	Rackliffe	McCune8	McCune12	McCune16	McCune20
v_f	0.65	0.44	0.42	0.44	0.43
$\rho \left[\frac{\text{lb.}}{\text{in.}^3} \left(\frac{\text{kg}}{\text{m}^3}\right)\right]$	0.049 (1360)	0.0517 (1431)	0.0521 (1443)	0.0517 (1431)	0.0519 (1437)
E_z [ksi (GPa)]	23300 (161)	13200 (90.7)	12600 (86.7)	13200 (90.7)	12900 (88.7)
E_θ [ksi (GPa)]	966 (6.66)	645 (4.45)	628 (4.33)	645 (4.45)	636 (4.39)
E_r [ksi (GPa)]	966 (6.66)	645 (4.45)	628 (4.33)	645 (4.45)	636 (4.39)
$\nu_{z\theta}$	0.32	0.33	0.33	0.33	0.33
ν_{zr}	0.32	0.33	0.33	0.33	0.33
$\nu_{\theta r}$	0.33	0.33	0.33	0.33	0.33
$G_{z\theta}$ [ksi (GPa)]	432 (2.98)	266 (1.83)	257 (1.77)	266 (1.83)	261 (1.80)
G_{zr} [ksi (GPa)]	432 (2.98)	266 (1.83)	257 (1.77)	266 (1.83)	261 (1.80)
$G_{\theta r}$ [ksi (GPa)]	364 (2.51)	243 (1.67)	236 (1.63)	243 (1.67)	239 (1.65)

Table 4 Geometric Parameters of Experimental Specimens

Specimen	L [in. (m)]	N_{t_L}	N_{t_H}	r_L [in. (mm)]	r_H [in. (mm)]	N_b	b [in. (cm)]	D [in. (cm)]
Rackliffe1	104 (2.64)	9	4	0.029 (0.743)	0.019 (0.495)	24	4.33 (11.0)	5.9 (15.0)
Rackliffe2	116 (2.94)	11	3	0.032 (0.821)	0.017 (0.429)	27	4.33 (11.0)	5.9 (15.0)
Rackliffe3	110 (2.80)	11	3	0.032 (0.821)	0.017 (0.429)	44	2.50 (6.35)	5.9 (15.0)
Rackliffe4	114 (2.89)	11	3	0.032 (0.821)	0.017 (0.429)	53	2.17 (5.51)	5.9 (15.0)
McCune8	14.1 (0.358)	8	4	0.064 (1.62)	0.045 (1.14)	5	2.84 (7.21)	5.0 (12.7)
McCune12	14.1 (0.358)	12	4	0.080 (2.03)	0.046 (1.17)	5	2.84 (7.21)	5.0 (12.7)
McCune16	14.1 (0.358)	16	4	0.090 (2.29)	0.045 (1.14)	5	2.84 (7.21)	5.0 (12.7)
McCune20	14.1 (0.358)	20	4	0.102 (2.58)	0.046 (1.17)	5	2.84 (7.21)	5.0 (12.7)

C. Finite Element Modeling

FE analyses were developed using the programs IsoTruss.exe and ANSYS WorkBench (versions 19.1 and R2). The WorkBench platform employs ANSYS SpaceClaim to define the structures' geometry and ANSYS Mechanical to generate the mesh, define constraints and load criteria, and solve the mathematical model. Static structural analyses were performed to predict the axial stiffness of the specimens tested by Rackliffe et al. and McCune. Eigenvalue buckling analyses were performed on the specimens tested by Rackliffe et al. to predict the critical buckling loads and modes.

1. Pre-processing

The pre-processing of the FE model includes four main components, summarized herein: geometry, mesh generation, boundary conditions, load criteria, and analysis type. The geometry of the IsoTruss structure is generated in the application Isotruss.exe. This program uses the inputs of bay length, number of bays, overall length, and number of nodes to create a wireframe structure based on the geometric patterns of IsoTruss structures. The wireframe is exported as a *.dxf CAD file and uploaded into ANSYS SpaceClaim (ASC). Within ASC, the wireframe geometry is converted into beam elements with the corresponding cross-sectional dimensions (see Table 4). The connectivity of the individual strut components is merged by defining the component topology as 'shared'.

The geometry is transferred to ANSYS Mechanical where the FE mesh is generated and boundary conditions are defined. Figure 1 provides data from a mesh refinement study, demonstrating how the critical buckling load predicted by the model is affected by increasing the coarseness of the FE mesh. The percent deviation of the critical buckling load was calculated relative to a standard mesh density of 5.08 in.$^{-1}$ (200 m^{-1}). A coarse mesh of 0.25 in.$^{-1}$ (10 m^{-1}) was used in the current study to reduce computation time and expense. The refinement study suggests that the coarse mesh can deviate approximately 2.7% from the standard, fine mesh.

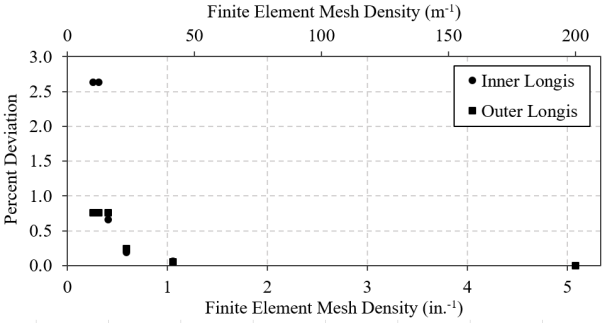

Fig. 1 Percent deviation vs. FE mesh density. ***(Copyright Brigham Young University, used with permission).***

The final step of pre-processing is to define boundary and loading conditions. The boundary conditions of the global truss are defined as fixed-free by fixing the nodes at one end (both the longitudinal and helical members). The uniaxial load is defined as a remote force, applied to the nodes of the longitudinal members on the opposite end of the structure. The remote force acts as a rigid load, distributed uniformly to the members. The remote force allows the end of the structure to deflect laterally during global buckling, but constrains the nodes as if the load were applied on a top plate.

2. Static Structural Analysis

After pre-processing, a static structural analysis is performed in ANSYS Mechanical to evaluate the axial stiffness. The loading is applied in ten steps, and the displacement is plotted against the force reaction to produce a load-displacement curve. The slope of this curve is the FE axial stiffness that is verified with mechanics calculations and validated with the experimental results.

3. Eigenvalue Buckling Analysis

The settings of the eigenvalue buckling model are programmed to derive the lowest five buckling modes and corresponding load multipliers. The critical buckling load is calculated from the load multiplier and the ultimate load applied in the analysis. The ultimate loads documented by McCune and Rackliffe et al. are used to prescribe the compression force in the FE model (see Table 6). The pre-stress environment of the eigenvalue buckling model is defined by the preceding static structural analysis.

D. Verification of FE Model using Mechanics

The axial stiffness, K_z, and critical buckling loads that are predicted by the FE models are verified with analytical expressions. Equation 1 predicts the axial stiffness from the modulus in the principal direction, E_z, the overall length of the IsoTruss structure, and the cumulative cross-sectional area of the longitudinal members.

$$K_z = \frac{E_z \cdot (N \cdot A_L)}{L} \tag{1}$$

Global buckling is predicted analytically with the Euler buckling equation for column buckling provided in Eq. 2. The boundary conditions of the column are defined as fixed-free, therefore, the boundary constraint coefficient, μ_g, is 2.0.

$$\begin{aligned} P_g &= \frac{\pi^2 \cdot E_z \cdot I_g}{(\mu_g \cdot L)^2} \\ \mu_g &= 2.0 \end{aligned} \tag{2}$$

The global moment of inertia can be calculated using two methods. The first method is presented by Winkel [1], and uses Eq. 3 with moment of inertia coefficients, c, derived for IsoTruss structures with inner or outer longitudinal (long.) members (see Table 5). The second method is presented by Sui et al., and uses Eq. 4. The methods are compared by Opdahl [6] for 8-node IsoTruss structures and produce the same result. The method presented by Winkel is implemented in the calculations presented herein.

$$I_g = c \cdot A_L \cdot R^2 \tag{3}$$

Table 5 Moment of Inertia Coefficients [1]

Nodes	6	7	8	9	10	11	12
Inner Long.	1	1.676	2.343	2.990	3.618	4.228	4.823
Outer Long.	3	3.5	4	4.5	5	5.5	6

$$\begin{aligned} I_g &= 4 \cdot \pi \cdot r_L^2 \cdot (d_1^2 + d_2^2) \\ d_1 &= R \cdot \sin(\theta) \\ d_2 &= R \cdot \cos(\theta) \cdot \tan(0.5 \cdot \theta) \end{aligned} \tag{4}$$

The analytical expression used to predict local/shell-like buckling is based on the derivation suggested by Sui et al. [5] and re-derived by Opdahl [6]. Shell-like buckling has a wavelength of two bays, and is localized to a single longitudinal segment that is intersected by helical struts within the buckling wavelength. The critical shell-like buckling load is calculated from the analytical expression provided in Eq. 5 for reference.

$$\begin{aligned} P_{sb} &= \frac{N \cdot \pi^2 \cdot E_z \cdot I_L}{(\mu_{sb} \cdot b)^2} \\ \frac{1}{\mu_{sb}^2} &= 1 + \frac{2 \cdot D_X \cdot l_1 \cdot \delta_2}{b \cdot E_z \cdot I_L} + \frac{2 \cdot D_X \cdot \delta_2 \cdot \sin\left(\frac{\pi \cdot l_1}{b}\right)}{\pi \cdot E_z \cdot I_L} \\ D_X &= \frac{E_X \cdot (2 \cdot r_H)^3}{12 \cdot (1 - \nu^2)} \\ E_X &= 2 \cdot \frac{E_z \cdot A_H}{(2 \cdot \delta_2) \cdot (2 \cdot r_H)} \cdot \sin^4(\phi) \end{aligned} \tag{5}$$

E. Validation of FE Model using Experimental Data

Table 6 summarizes the experimental data that is used to validate the FE model. The effective stiffness moduli, E_s, of the Rackliffe specimens were taken from the slopes of the stress-strain curves generated from the experimental test data. The effective stiffness moduli of the McCune specimens were calculated from the axial area, length, and average stiffness, K, reported by McCune in Table 4.5 [3]. The average modulus of elasticity reported by McCune in Table 5.4 [3] are less than 1% different than those shown in Table 6, except for the McCune16 specimen. The effective stiffness modulus reported in Table 6 for McCune16 is -5.6% different relative to the average modulus reported by McCune. The 'Axial Area' is the cumulative cross-sectional area of the eight longitudinal members (i.e., $N \cdot A_L$). The cross-sectional area of a single longitudinal member is calculated from the number of tows per longitudinal member (see Table 4) and the nominal fiber volume fraction (see Table 3).

Table 6 Previous Experimental Results [3] [4]

Specimen	E_s [ksi (GPa)]	Axial Area [in.^{2} (mm^2)]	K_z [kip/in. (kN/mm)]	P_{ult} [lb. (kN)]	Failure Mode
Rackliffe1	4610 (31.8)	0.0215 (13.9)	0.955 (0.167)	126 (0.560)	Local Buckling
Rackliffe2	8960 (61.8)	0.0263 (16.9)	2.03 (0.356)	135 (0.602)	Local Buckling
Rackliffe3	6420 (44.2)	0.0263 (16.9)	1.53 (0.268)	266 (1.18)	Global Buckling
Rackliffe4	5810 (40.1)	0.0263 (16.9)	1.34 (0.235)	251 (1.12)	Global Buckling
McCune8	8820 (60.8)	0.102 (65.8)	63.8 (11.2)	3600 (16.0)	Crushing
McCune12	7790 (53.7)	0.160 (103)	88.4 (15.5)	5380 (23.9)	Crushing
McCune16	8230 (56.7)	0.204 (132)	119 (20.8)	7920 (35.2)	Crushing
McCune20	8710 (60.1)	0.259 (167)	160 (28.0)	10400 (46.1)	Crushing

V. Results and Discussion

This section presents the axial stiffness and buckling results of the FE models and discusses their correlations with mechanics calculations and experimental data. These correlations are used to determine the effectiveness of the FE models in predicting the total deflection, buckling loads, and buckling modes of IsoTruss structures under uniaxial compression.

Five FE models were tested with various geometric and material properties to determine the parameters that would accurately predict the results of the experimental testing. The difference of the FE results relative to the analytical (i.e., Mechanics or Mech.) predictions and the experimental (i.e., Exp.) results were calculated using Eq. 6.

$$\text{Relative Difference} = \frac{\text{FE} - \text{Mech./Exp.}}{\text{Mech./Exp.}} \cdot 100 \quad (6)$$

Table 7 provides a summary of the FE models and the corresponding input parameters (i.e., the radii of the longitudinal and helical members and the material properties that include Young's modulus, Poisson's ratio, and the shear modulus). The input parameters of each model are either nominal or effective values. The 'nominal radii' were calculated from the reported number of tows in each member, the fiber volume fraction, and the area of a single tow. The 'nominal material properties' refer to the values that were calculated from micromechanics equations [8], and are shown in Table 3. The 'effective material properties' of FE Models C, D, and E are explained in greater detail in the subsequent sections. The 'measured radii' of Model B were measured physically from an experimental specimen. The results from FE Model B did not contribute to the conclusions of this study, and are therefore omitted.

Table 7 FE Models and Corresponding Parameters

Model ID	Radii	Material Properties (E_x)
A	Nominal	Nominal (Table 3)
B	Measured	Nominal (Table 3)
C	Nominal	Effective per Axial Stiffness (Table 6)
D	Nominal	Effective per Global Buckling Load (E_z = 142 GPa)
E	Nominal	Effective per Bay Buckling Load (E_z = 185 GPa)

A. Axial Stiffness

1. FE Model A

FE Model A implements the nominal length, nominal radii, and nominal material properties. The nominal length and nominal radii are based on the measurements, number of tows, and fiber volume fractions reported by Rackliffe et al. and McCune (see Table 4). Table 8 presents the theoretical stiffness calculated from the mechanics equation, Eq. 1, and the stiffness predicted by FE Model A.

Table 8 Axial Stiffness from Mechanics and FE Model A

	Axial Stiffness [kip/in. (kN/mm)]		FE Dif. Relative to	
Specimen	**Mech.**	**FE**	**Mech.**	**Exp.**
Rackliffe1	4.82 (0.845)	4.81 (0.843)	-0.24%	404%
Rackliffe2	5.24 (0.918)	5.23 (0.916)	-0.16%	157%
Rackliffe3	5.57 (0.975)	5.56 (0.973)	-0.20%	262%
Rackliffe4	5.33 (0.933)	5.32 (0.931)	-0.20%	296%
Average	5.24 (0.918)	5.23 (0.916)	-0.20%	280%
Std. Dev.	0.27 (0.047)	0.27 (0.047)	0.03%	87.9%
McCune8	95.2 (16.7)	95.7 (16.8)	0.58%	50.1%
McCune12	143 (25.0)	143 (25.0)	0.11%	61.6%
McCune16	190 (33.3)	189 (33.1)	-0.69%	58.9%
McCune20	236 (41.4)	237 (41.6)	0.45%	48.4%
Average	166 (29.1)	166 (29.1)	0.11%	54.7%
Std. Dev.	52.8 (9.24)	52.7 (9.23)	0.49%	5.63%

The average total deformation predicted by the FE models for the Rackliffe specimens was less than 1% different than that calculated from mechanics. When compared to the total deformation reported in the experiment, the average difference was 280%, with a standard deviation of 87.9%. Rackliffe et al. also acknowledged the large discrepancy between FE predictions and experimental results, attributing these differences to manufacturing and developmental factors. The discrepancy can also be attributed to the limitations of the micromechanics equations used to calculate the nominal properties.

Another possible source of decreased stiffness exhibited in the experimental testing could be the rotation of longitudinal struts within each bay, represented in Fig. 2. If the maximum deflection, δ_{max}, was distributed among all the bays, N_b, the average deflection per bay would be $4.12 \cdot 10^{-3}$ in. (0.105 mm). This local deflection corresponds to an average of 2.91° of rotation, γ, within each bay:

$$\gamma = \arccos\left(\frac{b - \frac{\delta_{max}}{N_b}}{b}\right) \tag{7}$$

Incorporating the local strut rotation of the bays in the FE model could enhance the accuracy of the FE model in predicting the experimental behavior of the specimens.

On the other hand, the axial stiffness predicted by FE Model A for McCune's specimens were, on average, 54.7% different than the axial stiffness exhibited in the experiment. While this is not an accurate prediction of the total displacement, the average standard deviation was 5.63%, showing greater precision than the Rackliffe models. The McCune structures were smaller and manufactured with more consistent methods and geometries than those constructed by Rackliffe et al. This implies that as specimens are manufactured with greater consistency, a more accurate prediction of the total deformation can be made using FE models. The effective stiffness modulus, based on experimental data, can be implemented in FE models to produce an accurate and precise prediction of total deflection. Figure 3 is a plot of the effective stiffness modulus of McCune's samples (demonstrated during experimental testing) versus the nominal modulus calculated from micromechanics. It suggests that the correlation factor that should be applied to the nominal modulus is approximately 0.65, to match the 8-node compression specimens tested by McCune.

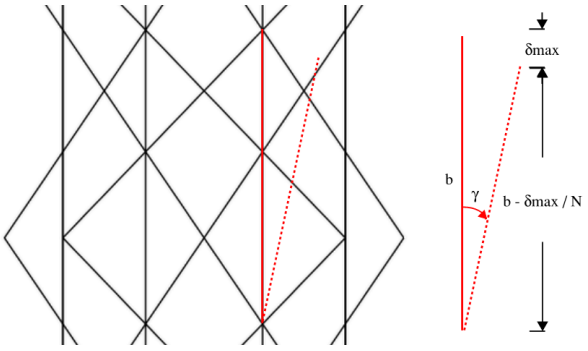

Fig. 2 Potential rotation of the longitudinal strut within each bay (not to scale). ***(Copyright Brigham Young University, used with permission).***

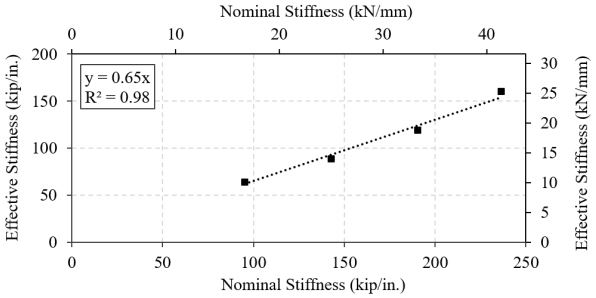

Fig. 3 Effective stiffness vs. nominal stiffness of McCune specimens. ***(Copyright Brigham Young University, used with permission).***

2. FE Model C

FE Model C was implemented to explore how an FE model could be defined to accurately predict the axial stiffness demonstrated by the Rackliffe experiments. Each Rackliffe specimen was modeled using the nominal length, nominal radii, and effective material properties. The effective material properties were derived from the effective moduli of elasticity, E_s, that were extracted from stress-strain curves generated from experimental data and are documented in Table 6. The axial stiffness predicted by FE Model C and by the mechanics equation, Eq. 1, are presented in Table 9.

The average difference of the FE predictions of axial stiffness relative to the predictions from mechanics is once again less than 1%. The difference relative to the experimental data was decreased from 280% to -0.83%, with a standard deviation of 0.50%. This analysis demonstrates that an accurate prediction of the total deformation can be made by adjusting the nominal material properties by a correlation factor to account for manufacturing inconsistencies, imperfections in the apparatus, and/or limitations of the micromechanics equations. It also implies that Eq. 1 is an accurate representation of the stiffness of IsoTruss structures under uniaxial compression. Additional studies could be performed to find correlations between the correlation factors and the structural design parameters such as the bay length, total length, and fiber volume fraction.

Table 9 Axial Stiffness from Mechanics and FE Model C

	Axial Stiffness [kip/in. (kN/mm)]		FE Dif. Relative to	
Specimen	**Mech.**	**FE**	**Mech.**	**Exp.**
Rackliffe1	0.954 (0.167)	0.951 (0.167)	-0.29%	-0.42%
Rackliffe2	2.01 (0.352)	2.01 (0.352)	-0.17%	-1.23%
Rackliffe3	1.53 (0.268)	1.53 (0.268)	-0.20%	-0.26%
Rackliffe4	1.32 (0.232)	1.32 (0.232)	-0.19%	-1.42%
Average	1.45 (0.254)	1.46 (0.256)	**-0.21%**	**-0.83%**
Std. Dev.	0.38 (0.067)	0.38 (0.067)	**0.05%**	**0.50%**

B. Eigenvalue Buckling

1. FE Model C

An eigenvalue buckling analysis was performed on each Rackliffe specimen to find a correlation between the critical buckling load predicted by FE methods and that exhibited in experimental testing. The first buckling analysis was performed using the effective material properties from the FE Model C static structural analysis. This model severely under-estimated the buckling capacity of the specimens, with an average difference of -72.5% relative to the experimental data. Table 10 presents the buckling loads predicted from FE Model C and from the mechanics expressions, Eq. 2 and Eq. 5. Table 10 also provides the difference of the FE predictions relative to the mechanics predictions and experimental results. The FE predictions were less than 3% different than the mechanics predictions when global buckling governed, however, there was greater deviation when local buckling governed.

Despite the disparity between the predicted and experimental buckling *loads*, FE Model C accurately predicted the experimental buckling *modes* of each Rackliffe specimen, except Rackliffe3. One possible reason for the discrepancy is that Rackliffe3 was constructed with a bay length of 2.5 in. (64 mm). According to Rackliffe [7], the IsoTruss structures designed within the specified design space that have a bay length greater than 2.5 in. will fail in local buckling, whereas structures with a bay length less than 2.5 in. will fail in global buckling. Since the bay length of Rackliffe3 is the transitional length between local and global buckling, it is not unreasonable for either failure mode to be predicted.

Table 10 Critical Buckling Loads from Mechanics and FE Model C

	Buckling Load [lb. (N)]		FE Dif. Relative to		Predicted Buckling Mode		
Specimen	**Mech.**	**FE**	**Mech.**	**Exp.**	**Mech.**	**FE**	**Exp.**
Rackliffe1	12.4 (55.3)	21.7 (96.5)	74.6%	-82.8%	Local	Local	Local
Rackliffe2	33.7 (150)	45.6 (203)	35.1%	-66.3%	Local	Local	Local
Rackliffe3	70.3 (313)	82.0 (365)	16.6%	-69.1%	Local	Local	Global
Rackliffe4	72.5 (323)	70.9 (315)	-2.16%	-71.7%	Global	Global	Global
Average	47.2 (210)	55.1 (245)	**31.0%**	**-72.5%**	-	-	-
Std. Dev.	25.3 (113)	23.4 (104)	**28.3%**	**6.26%**	-	-	-

2. FE Models D and E

Two additional models (i.e., FE Models D and E) were developed to find a correlation between the critical buckling loads predicted by FE methods and those demonstrated in experimental testing. The effective material properties used in FE Models D and E were derived from the load multipliers and material properties of FE Model C by the following process. Eq. 8 was used to calculate a new E_z for each specimen by dividing the E_z from FE Model C by the corresponding load multiplier, λ, predicted by the eigenvalue buckling analysis. The new E_z is referred to as the effective buckling modulus, E_b, whereas the E_z from FE Model C is referred to as the effective stiffness modulus, E_s. The remaining material properties were calculated from the new E_z using micromechanics.

$$E_b = \frac{E_s}{\lambda} \tag{8}$$

The average effective buckling modulus of Rackliffe3 and Rackliffe4 was 20600 ksi (142 GPa) with a standard deviation of 120 ksi (0.83 GPa). This average modulus was used to derive the remaining material properties for FE Model D. The average effective buckling modulus of Rackliffe1 and Rackliffe2 was 26800 ksi (185 GPa) with a standard deviation of 119 ksi (0.82 GPa). This average modulus was used to derive the remaining material properties for FE Model E. The results from FE Models D and E are presented in Table 11 and Table 12, respectively. These tables also include the mechanics predictions calculated with Eq. 2 and Eq. 5.

Table 11 Critical Buckling Loads from Mechanics and FE Model D

	Buckling Load [lb. (kN)]		FE Dif. Relative to		Predicted Buckling Mode		
Specimen	**Mech.**	**FE**	**Mech.**	**Exp.**	**Mech.**	**FE**	**Exp.**
Rackliffe3	226 (1.00)	258 (1.15)	14.5%	-2.71%	Local	Local	Global
Rackliffe4	257 (1.14)	251 (1.12)	-2.52%	0.02%	Global	Global	Global
Average	241 (1.07)	255 (1.13)	**5.99%**	**-1.34%**	-	-	-
Std. Dev.	15.8 (0.070)	3.86 (0.017)	**8.52%**	**1.37%**	-	-	-

The relative differences between the FE predictions and the experimental data are, on average, -1.34% and -1.27% for FE Model D and FE Model E, respectively. The differences relative to mechanics predictions are less than 3% when global buckling governs, however, the deviation varies significantly between local buckling (i.e., shell-like buckling) predictions. FE Models D and E predict the critical buckling load with greater accuracy than Model C with respect to experimental data. Additional exploration is needed to increase the accuracy of the prediction of shell-like buckling from mechanics. The standard deviation between the predictions of FE Model E and mechanics calculations is 18.8%.

Predictions from FE Models D and E demonstrate

Table 12 Critical Buckling Loads from Mechanics and FE Model E

	Buckling Load [lb. (N)]		FE Dif. Relative to		Predicted Buckling Mode		
Specimen	**Mech.**	**FE**	**Mech.**	**Exp.**	**Mech.**	**FE**	**Exp.**
Rackliffe1	72.3 (322)	123 (549)	70.7%	-2.02%	Local	Local	Local
Rackliffe2	101 (450)	135 (599)	33.1%	-0.52%	Local	Local	Local
Average	86.7 (386)	129 (574)	**51.9%**	**-1.27%**	-	-	-
Std. Dev.	14.4 (64.1)	5.63 (25.0)	**18.8%**	**0.75%**	-	-	-

significant improvement from FE Model C, reducing the relative difference from -72.5% to -1.34% and -1.27%. This demonstrates that the FE model is viable in predicting the critical buckling load when the modulus is adjusted to account for manufacturing imperfections and micromechanics limitations. The correlation factors of 0.88 and 1.15 were applied to the nominal modulus (i.e., 23300 ksi or 161 GPa), to calculate the effective buckling moduli of FE Models D and E, respectively. The adjustment factors 0.88 and 1.15 may depend on the failure mode (i.e., global versus shell-like buckling) or the geometric parameters of the IsoTruss structure (i.e., 2.17- and 2.50-inch bay length versus 4.33-inch bay length). Additional research is needed to determine the interrelations between geometric parameters and the correlation factors.

VI. Conclusion

A finite element (FE) model is presented to predict the total deflection and critical buckling load of IsoTruss structures subject to uniaxial compression. The model is verified with traditional mechanics calculations and validated with experimental data from preceding studies. The FE predictions of total deflection are within 1% of those predicted with traditional mechanics, but underestimate the deflection exhibited by experimental testing. The total deflection from experimentation can be accurately predicted with mechanics and the FE model if the nominal modulus of elasticity (calculated with micromechanics) is changed to an effective modulus using a correlation factor. The correlation factor accounts for imperfections in the physical specimens, imperfections in the testing apparatus, an overestimated fiber volume fraction, and/or limitations of the micromechanics equations. The factor is approximately 0.65 for the specimens tested by McCune. The correlation factors for the specimens tested by Rackliffe et al. had significant variation between samples due to manufacturing inconsistencies.

The critical buckling loads predicted in the FE model are within 3% of the predictions from Euler buckling calculations when global buckling is the governing buckling mode. When shell-like buckling governs, there is greater variation in the predictions from the FE model and those from the mechanics equation derived by Opdahl [6]. The discrepancies between FE predictions and the analytical equation are explored further by Opdahl and Jensen [9] to identify potential sources of deviation. The buckling models also use a correlation factor to accurately predict the buckling loads exhibited in experiment. The factors fluctuate depending on the geometry and failure mode of the distinct configuration. More research is needed to determine how the correlation factors vary with respect to the design parameters of the IsoTruss structure.

The finite element models predicted the same critical buckling modes as the analytical expressions for each tested configuration. The FE and analytical methods predicted the same critical buckling modes exhibited in experiment except for Rackliffe3. The Rackliffe3 specimen has a bay length of 2.5 in. (64 mm). This particular bay length has been identified previously by Rackliffe as the transition between local and global buckling for configurations within the design space tested.

In addition to enhancing the accuracy of the finite element model, improvements are needed to more accurately predict shell-like buckling via engineering mechanics. The method presented by Opdahl [6] is discussed by Opdahl and Jensen [9] to determine why there is variation in the results and how to improve the accuracy and precision. With a greater understanding of the mechanics of shell-like buckling, a model can be implemented that will consistently predict the governing buckling mode. While shell-like buckling and global buckling were the only buckling modes demonstrated by the FE models of this study, longitudinal strut buckling is a potential buckling mode if the helical members are robust enough to constrain the longitudinal members.

The model developed in this study is an effective tool for the numerical analysis of IsoTruss structures in subsequent studies. It provides a framework for dimensional and optimization analyses of IsoTruss structures, including a method to gauge the relative performance of novel configurations of IsoTruss structures such as those with outer longitudinal members.

Acknowledgments

This research was supported by the Utah NASA Space Grant Consortium. The authors express their gratitude to the Consortium and all associated personnel.

References

[1] Winkel, L. D., "Parametric Investigation of IsoTruss™ Geometry Using Linear Finite Element Analysis," M.S. Thesis, Brigham Young University, 2001.

[2] Francom, L. R., and Jensen, D. W., "Three-dimensional Iso-Truss structure," 1999. US Patent 5,921,048.

[3] McCune, A. M., "Tension and Compression of Carbon/Epoxy IsoTruss™ Grid Structures," M.S. Thesis, Brigham Young University, 2001.

[4] Rackliffe, M. E., Jensen, D. W., and Lucas, W. K., "Local and global buckling of ultra-lightweight IsoTruss® structures," *Composites Science and Technology*, Vol. 66, No. 2, 2006, pp. 283–288. https://doi.org/10.1016/j.compscitech.2005.04.038.

[5] Sui, Q., Fan, H., and Lai, C., "Failure analysis of 1D lattice truss composite structure in uniaxial compression," *Composites Science and Technology*, Vol. 118, 2015, pp. 207–216. https://doi.org/10.1016/j.compscitech.2015.09.003.

[6] Opdahl, H. B., "Investigation of IsoTruss Structures in Compression Using Numerical, Dimensional, and Optimization Methods," M.S. Thesis, Brigham Young University, 2020.

[7] Rackliffe, M. E., "Development of Ultra-lightweight IsoTruss™ Grid Structures," M.S. Thesis, Brigham Young University, 2002.

[8] Kollar, L. P., and Springer, G. S., *Mechanics of Composite Structures*, Cambridge University Press, 2003.

[9] Opdahl, H. B., and Jensen, D. W., "Dimensional Analysis of Shell-like Buckling in IsoTruss® Structures using Numerical Methods," *AIAA Scitech 2021 Forum*, 2021, p. 0700. https://doi.org/10.2514/6.2021-0700.